Spectroscopic investigation of highly transient pinch plasmas

K. Bergmann,[1] O. N. Rosmej,[2] F. B. Rosmej,[3] A. Engel,[1] C. Gavrilescu,[4] W. Neff,[5] and R. Lebert[1]
[1] *Lehrstuhl für Lasertechnik, Steinbachstrasse 15, D-52074 Aachen, Germany*
[2]*MISDC VIIFTRI, 141570 Mendeleevo, Moscow, Russia*
[3]*Institut für Experimentalphysik V, Ruhr-Universität Bochum,Universitätsstrasse 150, D-44780 Bochum, Germany*
[4]*University of Iasi, Copou 11, 6600-Iasi, Romania*
[5]*Fraunhofer Institut für Lasertechnik, Steinbachstrasse 15, D-52074 Aachen, Germany*
(Received 18 December 1996)

The temporal evolution of neon pinch plasmas, generated in a 2 kJ plasma focus device, has been investigated by x-ray spectroscopic methods for two sets of device parameters. These two sets lead to characteristic differences of the *K*-shell emission. Stationary models are shown to fail to explain the experimental observations even qualitatively. Transient spectra analysis shows that the characteristic differences observed can be referred to different transient modes of plasma dynamics. The spectra analysis includes beside resonance lines also dielectronic satellites and recombination continua. The results concerning the development of the plasma parameters achieved by the spectra modeling are supported by independent measurements of the time resolved *K*-shell emission and by optical streak images of the pinch plasma dynamics, which confirms the reliability of the transient spectroscopic analysis presented. [S1063-651X(97)12510-7]

PACS number(s): 52.25.Nr, 52.55.Ez

I. INTRODUCTION

Dense, high-*Z* plasmas with electron densities of about 10^{20} cm^{-3} and temperatures of several 100 eV are intense sources of pulsed radiation in the soft x-ray range (about 50 eV–5 keV photon energy) and can be generated with laboratory scale devices. Various devices for the generation of such plasmas are under investigation: laser plasmas, *Z*-pinch, gas puffs, capillary discharges, vacuum sparks, or the plasma focus. In this paper the plasma focus device is under discussion [1].

Typical time scales of collisional and radiative processes of such plasmas are of the same order of magnitude as the lifetime, which is of about several nanoseconds. The nature of the plasma development is therefore essentially transient. The understanding of the various transient processes is of great importance for the specification according to different applications and their optimization. This knowledge allows, for example, the tailoring of flexible x-ray sources having special spectral characteristics concerning wavelength region or bandwidth demanded by a given application. Furthermore, the transient coupling in plasmas becomes of importance for scaling down the devices to lower currents in order to have tabletop size for laboratory applications. Especially for x-ray lasers based on a gas discharge [2–4] the understanding of the transient coupling of the plasma parameters and radiative processes is a necessary precondition for, e.g., scaling down to lower wavelengths.

For the plasma focus under investigation the full set of determining device parameters is accessible. The possibility to correlate uniquely the device parameters and the plasma parameters enables the deduction of scaling laws and optimization criteria.

The present paper deals with the experimental and theoretical investigation of the plasma dynamics. X-ray spectroscopic methods and transient spectra modeling for the interpretation of the experimental emission spectra have been employed.

The usual approach to the investigation of transient plasmas is obtaining the time-dependent plasma parameters from the magnetohydrodynamics (MHD) calculations and their subsequent use in a spectroscopic postprocessor (e.g., [1,5–10]), where often only a part of the spectral information like total yield or a few resonance lines is compared to experimental data.

In addition to *K*-shell resonance lines we also investigate in detail dielectronic satellite spectra and recombination continua. The transient spectra modeling presented is based on a few crude assumptions concerning the qualitative evolution of the plasma parameters, which are confirmed by time resolved measurements. The absolute values of the plasma parameters are estimated by comparing the calculated time integrated spectra to experimental highly resolved spectra. The overall spectra modeling is shown to deliver reliable information about the time-dependent plasma parameters. It is shown that for the phase of plasma decay dielectronic satellite spectra and photorecombination provide information about different possible modes of plasma decay. Time integrated spectra of transient neon pinch plasmas have been consistently interpreted.

II. EXPERIMENTAL SETUP AND PLASMA FORMATION

The experiments were carried out using a plasma focus of Mather type [11]. A schematic drawing is given in Fig. 1. The storage capacity ($C=36$ μF) is connected by a low inductance spark gap to the electrode system, which is embedded in a high-Z gas filling with pressures of several 100 Pa. The anode radius was $a=1$ cm. The inductance of the capacity bank, the electrical connections, and the switch are of about $L=20$ nH. The system is operated using a voltage between 8 kV and 12 kV leading to pinch currents in the

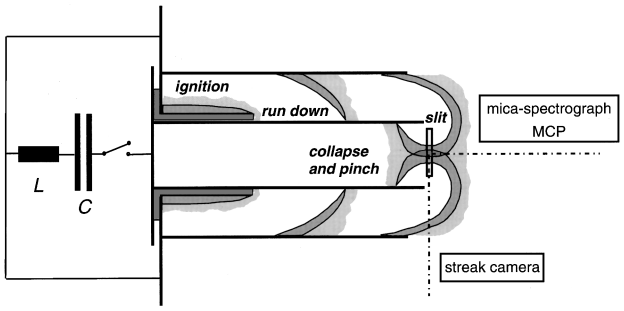

FIG. 1. Scheme of the plasma focus with the four phases of the discharge development. In addition, the region covered by the slit used in the optical streak measurements is shown schematically.

range of 200–300 kA. More details concerning the device are described elsewhere [12,21].

The current was measured using a calibrated magnetic probe which was positioned in the electrode system near the end of the anode. This enables a measurement of the local current going through the pinch plasma which was shown to be different from the total device current due to leakage currents above the anode. Details concerning the setup for the current measurements and the leakage current behavior are given in Ref. [12].

The typical electron densities of the pinch plasma are in the range of 10^{20} cm^{-3}, electron temperatures are of the order of several 100 eV. These parameters give rise to an intensive *K*-shell line emission, in particular those of the H-, He- and Li-like ionization stages.

The spectra of the neon pinch plasmas were taken by means of a cylindrically curved defocusing mica crystal positioned in axial direction (see Fig. 1). The curvature radius of the crystal was 1 cm. The distance between the plasma and the bent mica crystal ($2d=1.992$ nm) was 33 cm. To prevent visible light illuminating the detector (Fuji 80 x-ray film), a beryllium foil with thickness 12 μm was positioned between the pinch plasma and the crystal. The total spectral resolution, which is determined by that of the crystal (of about 1300) and a contribution due to the finite size of the source in the respective wavelength region (about 400 μm), is of about $\lambda/\Delta\lambda \simeq 900$.

Time resolved *K*-shell emission in axial direction (see Fig. 1) was investigated using a microchannel plate detector (MCP), which has a temporal resolving power better than 1 ns. The entrance of the MCP was covered by a 10 μm aluminum foil restricting the detected spectral range to wavelengths below 1 nm.

Images in the visible spectral regime of the collapsing and of the expanding pinch plasma were taken using a streak camera. A slit of 25 μm width was placed between the plasma and the optics of the streak camera in order to cut out a small region in axial direction allowing us to measure the collapsing and expanding plasma layer (see Fig. 1). In a distance of 2.5 mm to the end of the anode a region of about 100 μm width in axial direction is observed. The time resolution of the streak measurement is better than 0.5 ns.

The development of the discharge can be divided into four phases, which are also indicated in Fig. 1. In the first phase a sliding discharge builds up on the insulator after applying the voltage of the charged capacity to the electrode system. This sliding discharge leads to a homogeneous cylindrical plasma layer. In the second phase this layer is accelerated by Lorentz forces to the end of the anode collecting the neutral gas particles. Simultaneously the current rises to its maximum value during this second phase.

The last two phases are similar to a *Z*-pinch dynamics. The plasma layer is accelerated towards the axis and on reaching the axis the accumulated kinetic energy is converted into thermal energy leading to a dense and hot pinch plasma. The temperatures achieved lead to emission from highly charged ions. The process of thermalization of the ion kinetic energy goes in two steps. First the kinetic energy of the ions is converted to thermal energy of the ion gas. The kinetic energy of the collapsing electrons can be neglected because of their low mass. The electrons are heated by the hot ion gas.

The last two phases of the discharge determine the dynamics of the pinch plasma and the x-ray production. It can be shown that for the device under investigation three device parameters uniquely determine these two phases for a fixed element. These parameters are the current I_0 at the beginning of the compression phase, the number density of the neutral gas or the working gas pressure p and the radius of the anode a [13].

These device parameters can be correlated with the pinch plasma parameters. Based on similarity considerations, which are discussed in more detail in Ref. [13], the ion and electron temperatures achievable in the pinch plasma scale as $T_e \propto I_0^2/(pa^2)$. Keeping this parameter constant, i.e., discussing plasmas in equal temperature regimes, and assuming negligible radiative losses compared to the total energy input into the pinch plasma the ion density is expected to be proportional to the neutral gas pressure $n_i \propto p$.

The transient plasma dynamics is essentially determined by the confinement parameter $n_e\tau$, where τ is the lifetime of the pinch plasma. So by using different neutral gas pressures the confinement parameter can be varied as will be shown below.

III. X-RAY EMISSION OF NEON PINCH PLASMAS

Figures 2(a) and 2(b) show the *K*-shell emission lines of H-, He-, and Li-like neon ions taken at working gas pressures of 400 Pa ($I_0=260$ kA ± 10 kA) and 200 Pa ($I_0=250$ kA $\pm$ 10 kA), respectively. Figure 2(a) shows the H-like series $1s\ ^2S_{1/2}-np\ ^2P_{1/2,3/2}$ up to $n=6$ and the corresponding series of He-like ions $1s^2\ ^1S_0-1snp\ ^1P_1$ up to the series limit. The present spectral resolution permits the clear identification up to $1s^2\ ^1S_0-1s7p\ ^1P_1$. Also resolved are the He-like resonance *W* line $1s^2\ ^1S_0-1s2p\ ^1P_1$ and intercombination *Y* line $1s^2\ ^1S_0-1s2p\ ^3P_1$.

Besides the emission lines originating from single excited levels there are observed numerous screened resonance transitions originating from the double excited autoionizing levels $2lnl'$ and $1s2lnl'$. These double excited levels give rise to so-called dielectronic satellite spectra. For $n=2$ these dielectronic satellites are well separated from the $n=2$ resonance lines. Higher order satellites ($n \geqslant 3$) have two radiative decay channels:

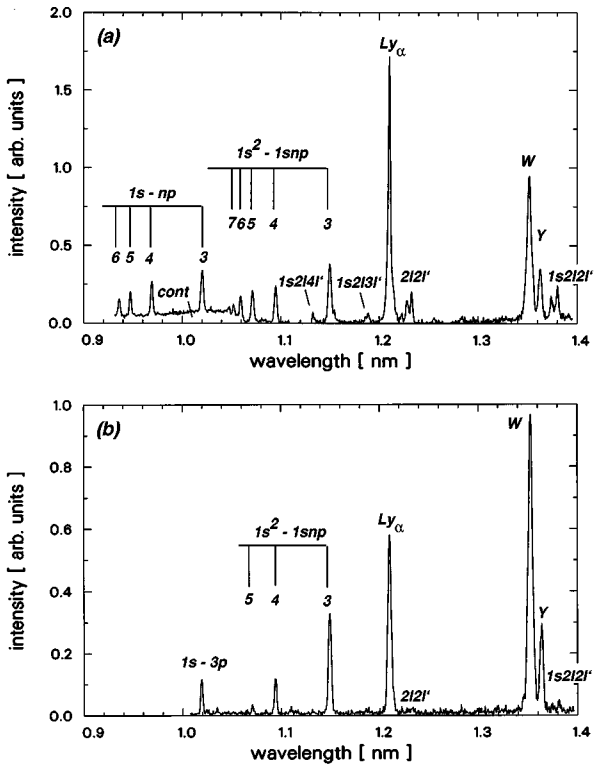

FIG. 2. (a) Experimental x-ray neon spectrum showing the 1s-np and $1s^2$-1snp series of H- and He-like ions together with its He-like and Li-like satellites for the 400 Pa case. (b) Experimental x-ray spectrum at 200 Pa neon pressure.

$$1s2lnl' \rightarrow \begin{cases} 1s^2nl' + \hbar\omega \\ 1s^22l + \hbar\omega. \end{cases} \tag{1}$$

The first channel gives rise to satellite transitions on the red wing of the He-like *W* line, which are not resolved. They result in a ''red'' asymmetry of the *W* line. The second decay channel is resolved from their respective resonance lines. In the spectrum of Fig. 2(a) the transitions $1s2lnl' - 1s^22l'$ are seen for $n=3,4$. The He-like autoionizing levels $2lnl'$ have similar decay channels resulting in a red asymmetry for the Ly$_\alpha$ line. However, for $n \geqslant 3$ the intensity is rather weak and can hardly be used for diagnostics. The observed resonance and satellite lines are well suited for the determination of plasma parameters (see, e.g., the review of Boiko *et al.* [14]).

The spectra taken at 200 Pa and 400 Pa [Figs. 2(a) and 2(b)] show characteristic differences in the line emission.

(1) Dielectronic satellite spectra and recombination continuum are practically absent for the 200 Pa discharge and rather strong for 400 Pa.

(2) The intensity ratio of the Ly$_\alpha$ to *W* line for the 400 Pa spectrum is much higher than for 200 Pa.

In a stationary treatment of the time integrated spectra conditions (1) and (2) contradict each other. To obtain very low satellite spectra, the temperature must be of about 400 eV. For such electron temperature, the emission in the Ly_α-line must exceed that of the *W* line by a factor of 2.5–4.5 for electron densities in the range of 10^{18}–10^{20}cm^{-3}. The experimentally observed ratio for the 200 Pa spectrum is, however, only 0.4. On the other hand, the high intense satellite spectra in the 400 Pa case [Fig. 2(a)] suggest an electron temperature of about 200 eV resulting in a Ly$_\alpha$ intensity much lower than that of the *W* line, just opposite to the experimental observation. We have investigated also various radiation transport effects (different effective photon path lengths, ionization balance shift). However, the principal discrepancies remain and cannot be resolved in a stationary treatment.

It will be shown below that a complete transient spectra analysis can resolve the discrepancies outlined above.

IV. TRANSIENT SIMULATION OF PLASMA DYNAMICS

Transient effects in the line formation become of increasing importance if the time scales for atomic processes are not small in comparison to the time scales for the change of the plasma parameters. E.g., if the plasma suffers a fast heating process the ion abundance and the line emission originating from different ionization levels do not correspond to the electron temperature. Both lag behind the electron temperature. An example for Li-like ions is given in Ref. [15]. In fast recombining plasmas we encounter opposite relations: the degree of ionization is higher compared to equilibrium conditions when the electron temperature decreases. During the time history of the pinch plasmas under investigation compression and expansion take place. We therefore meet both phenomena, which leave their marks in the emission spectra.

For the investigation of the transient line formation of the pinch plasma a collisional-radiative, metastable resolved, time dependent model has been employed [16]:

$$\frac{dn_j}{dt} = \sum_{i,i\neq j} W_{ij}n_i - \sum_{i,i\neq j} W_{ji}n_j, \tag{2}$$

where n_i are the atomic level populations, W_{ij} are the various collisional and radiative rate processes for the population and depopulation of the levels, namely, collisional excitation and deexcitation, ionization and three body recombination, dielectronic recombination and autoionization, and radiative recombination. Radiation transport effects have been taken into account by means of escape factors [17] and iteratively solving for the level populations. More details have been described elsewhere [16,18,19].

The interpretation of the plasma dynamics was carried out in the following way.

(1) Generation of time-dependent parameters $n_e(t)$ and $T_e(t)$ from a plasma bag model calculation and subsequent use of these parameters for the calculation of emission spectra solving the set of differential equations (2). In this frame Eqs. (2) can be considered as a postprocessor of the model calculations. The use of $n_e(t)$ and $T_e(t)$ implies the assumption of a single zone. However, detailed comparison of one- and two-dimensional modelings with those of a zero-dimensional approach have shown that the zero-dimensional model provides a reasonable characterization of the plasma evolution [20]. Details concerning the present plasma bag model are described elsewhere [21]. The plasma bag model describes the compression and the pinch phase in the framework of a quasi-one-dimensional model making use of a simplified geometry of the plasma layer and assuming a homogeneous density and temperature of ions and electrons. This

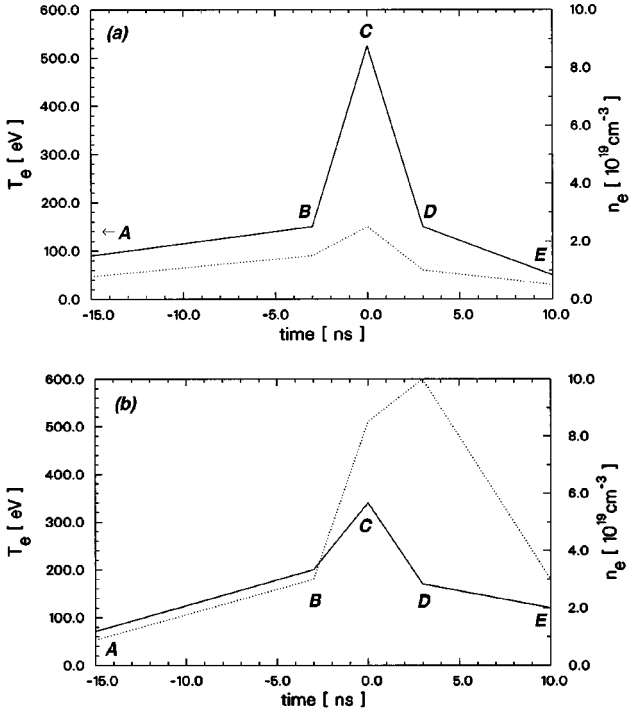

FIG. 3. Simplified parameter dependence of $T_e(t)$ (full) and $n_e(t)$ (dotted) which was used for the fitting of the emission spectra. The values at the instances A–E correspond to those given in Tables I and II for the 200 Pa case (a) and for the 400 Pa case (b). The parameter dependence for temperature and density from the plasma bag calculations does not differ essentially in its qualitative behavior but has different numerical values also given in Tables I and II.

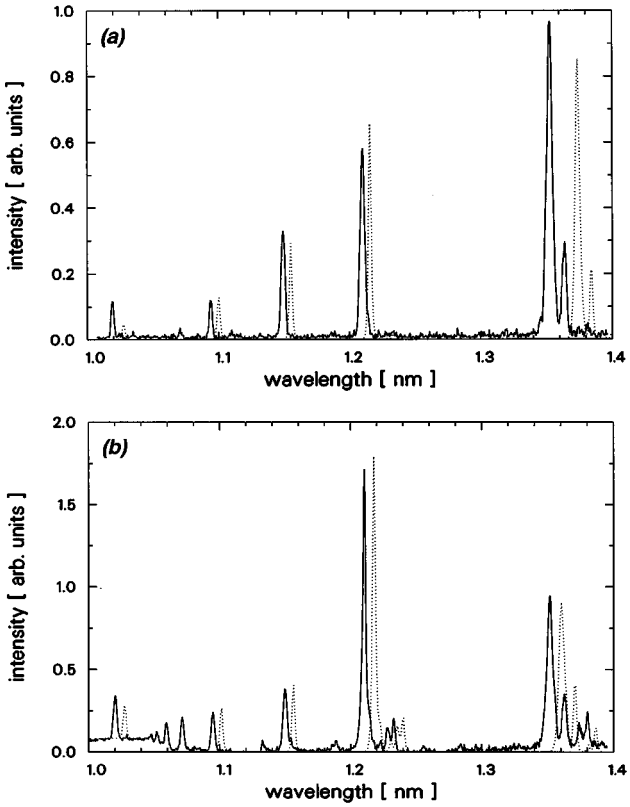

FIG. 4. (a) Theoretical spectrum fitting together with the experimental data for 200 Pa gas pressure. (b) Theoretical spectrum fitting together with the experimental data for 400 Pa gas pressure.

model includes the coupling of the device parameters to the hydrodynamic motion including acceleration of the plasma due to magnetic forces, shock heating at the boundary of the plasma layer to the neutral gas, thermalizing of kinetic energy in the pinch phase, heating of electrons by hot ions and Ohmic heating, and the influence of radiative processes on the plasma parameters. These processes are described in the zero-dimensional approach within the temporal evolution of electron density and temperature.

(2) The atomic structure of Eq. (2) includes resonance lines, forbidden transitions, and in a detailed manner the dielectronic satellite lines $1s2l2l'$-$1s^2 2l'$ and $2l2l'-1s2l'$ of Li- and He-like ions and the recombination continua. Theoretical emission spectra were therefore used for purely spectroscopic investigation of the plasma dynamics: $n_e(t)$ and $T_e(t)$ are regarded as ''test functions'' providing a theoretical spectrum to be comparable with the experimental one. Starting point for the test functions were the results obtained by the plasma bag calculations.

This method enables the theoretical investigation of different modes of plasma dynamics. Simultaneous fitting of many resonance and forbidden lines provides reliable information about time dependent plasma parameters and can be used for a refinement of the results of pure MHD calculations.

The emission spectra strongly depend on the principal behavior of the plasma parameters, namely, duration of compression and expansion together with the maximum values of T_e and n_e. Comparing the emission spectra resulting from the numerical $n_e(t)$ and $T_e(t)$ provided by plasma bag calculations with those of various testing functions allows us to use a simplified dependence, as shown in Fig. 3. A slow heating and compression phase ''*A*-*B*,'' a further short compression to maximum T_e and n_e ''*B*-*C*,'' a short expansion and cooling to medium plasma parameters ''*C*-*D*,'' and a long lasting cooling and expansion phase ''*D*-*E*.'' Proper selection of the T_e and n_e at the instants A–E leads to emission spectra which practically do not differ from those employing numerical values from the plasma bag calculations.

The phase *A*-*B* corresponds to the end of the compresion phase before the plasma layer reaches the axis. The fast increase in density and temperature *B*-*C* is due to the thermalizing of the kinetic ion energy and subsequent heating of electrons. With the additional internal energy of the kinetic ions the pinch plasma pressure exceeds the magnetic pressure which will lead to the expansion in the phases *C*-*D* and *D*-*E*.

TABLE I. Plasma parameters at the instants A–E indicated in Fig. 3 given by the plasma bag calculations. In parentheses are the corrected values, which lead to an improvement of the fitted spectrum in the 200 Pa case.

Parameter	*A*	*B*	*C*	*D*	*E*
T (ns)	-23	-3	0	3	10
T_e (eV)	50	150	650 (525)	150	50
$n_e(10^{19}\text{cm}^{-3})$	0.3	1.5	20 (2.5)	1.0	0.5

TABLE II. Plasma parameters at the instants A–E indicated in Fig. 3 given by the plasma bag calculations. In parentheses are the corrected values, which lead to an improvement of the fitted spectrum in the 400 Pa case.

Parameter	A	B	C	D	E
T ns	-16	-3	0	3	10
T_e (eV)	60	200	370 (340)	200 (170)	100 (120)
n_e (10^{19}cm^{-3})	0.7	3	30 (8.5)	15 (10)	3.0

Figures 4(a) and 4(b) show the total spectrum fitting of the 200 Pa and the 400 Pa experiment obtained with the parameter development given in Fig. 3 (higher series lines $1s$-np, $1s^2$-$1snp$ with $n>4$ have not been taken into the theoretical consideration). The numerical values for the plasma parameters n_e and T_e at the instants A–E used for the fittings are given in Tables I and II. These two tables contain the numerical values obtained from the plasma bag calculations and a set of corrected values resulting from the transient spectra modeling. For the fitted spectra shown in Figs. 4(a) and 4(b) the corrected values have been taken into account. The corrections will be discussed below in more detail. With both sets of plasma parameters a good agreement between experimental and theoretical results is obtained for the most essential spectral features: occurrence or absence of the recombination continua, lower intensity in the satellite lines for the 200 Pa case in comparison with the 400 Pa experiment, and the line ratios of the W line to the Ly$_\alpha$ line.

Tables III and IV summarize the most important experimental line intensity ratios together with the theoretical calculations of the ratios of the time integrated intensities:

$$\overline{I_K} = \int_{t_A}^{t_E} I_K(t)\,dt \tag{3}$$

for the emission line K. The $I_K(t)$ are determined from Eq. (3) using $I_K(t)=n_K(t)A\Theta(t)\hbar\omega$. A is the coefficient for spontaneous decay and $\Theta(t)$ the escape factor for radiation transport.

As the atomic model includes simultaneously levels of various ionization stages (boron-like till nucleus) the solution of Eqs. (2) provides also the time dependent ion abundance shown in Figs. 5(a) and 5(b). In the 200 Pa case the fast change of T_e and n_e in time does not permit the ion abundance to be in a stationary regime. The time to proceed ionization to the nucleus is too long, the plasma expands before the He-like ion abundance experiences a considerable depopulation: the confinement parameter $n_e\tau$ is too small to reach a stationary regime ($n_e\tau<5\times10^{10}$ cm^{-3}s) [18]. In a stationary regime ($n_e\tau>10^{12}$cm^{-3}s) with $T_e=550$ eV, $n_e=2\times10^{19}$cm^{-3}, and $L_{\rm eff}=0.7$ cm ($L_{\rm eff}$ is the effective photon path length obtained from experimental estimations and being in agreement with spectra modeling) the relative ion abundance would be $n(\text{nucleus})\simeq0.81$, $n(\text{H})\simeq0.18$, $n(\text{He})\simeq5\times10^{-3}$. So one would expect negligible W-line radiation that is in contradiction to the experimental results. The observed high W-line intensity compared to the Ly$_\alpha$ line is due to a long lifetime of the He-like ions with respect to the total lifetime of the pinch plasma.

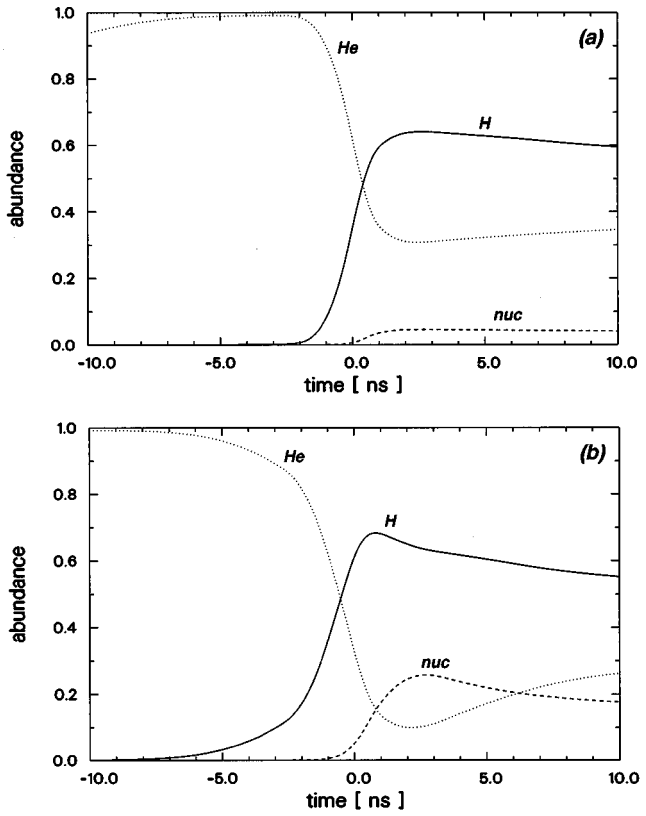

FIG. 5. (a) Time-dependent ion abundances for nucleus, H, and He, ground states obtained from the time-dependent plasma parameters as given in Table I for the 200 Pa gas pressure. (b) Time-dependent ion abundances for nucleus, H, and He, ground states obtained from the time-dependent plasma parameters as given in Table II for the 400 Pa gas pressure.

For the experiments with 400 Pa gas pressure we meet not only different plasma parameters at maximum compression but also a different regime due to a higher value of the confinement parameter. Although the temperature at maximum

TABLE III. Calculated and experimental line ratios of different transitions for the 200 Pa case.

Transition	Experimental ratio	Theoretical ratio
Ly$_\alpha$:W	0.45	0.49
W:Y	6.1	5.7
W:($1s^2$-$1s3p$)	4.8	4.4
Ly$_\alpha$:($1s-3p$)	5.4	13
J:Ly$_\alpha$	0.02	0.02

TABLE IV. Calculated and experimental line ratios of different transitions for the 400 Pa case.

Transition	Experimental ratio	Theoretical ratio
Ly$_\alpha$:W	1.14	1.07
W:Y	3.8	3.6
W:($1s^2$-$1s3p$)	3.8	3.7
Ly$_\alpha$:($1s-3p$)	7.7	7.8
J:Ly$_\alpha$	0.11	0.13

compression is considerably lower than for the 200 Pa experiment, the He-like ion abundance suffers a much higher depopulation due to a higher electron density and higher confinement parameter. The nucleus reaches a higher population. Figure 5(b) shows the time-dependent ion abundance for the 400 Pa gas pressure. We want to note that also for the 400 Pa gas pressure the stationary regime is not completely approached. For $T_e = 350$ eV, $n_e = 8 \times 10^{19}$ cm^{-3}, and $L_{\text{eff}} = 0.7$ cm one obtains the ion abundances $n(\text{nucleus}) \simeq 0.61$, $n(\text{H}) \simeq 0.36$, $n(\text{He}) \simeq 0.03$.

Taking the average over the time interval from t_B to t_E, where the K-shell emission is most intense, the He-like ion abundance for the 400 Pa experiment is lower than for the 200 Pa experiment. This is why the Ly$_\alpha$ intensity exceeds that of the W-line, although the temperature at maximum compression is lower than for the 200 Pa experiment.

Two-dimensional calculations of a plasma focus discharge show also a strong fall off in z direction [22]. Excitation rates for dielectronic capture $\langle \text{DC} \rangle$ and collisional excitation $\langle C \rangle$ for dielectronic satellites and resonance lines scale according to $\langle \text{DC} \rangle \propto n_{gr} n_e \exp(-E_s/T_e)/T_e^{3/2}$ and $\langle C \rangle \propto n_{gr} n_e \exp(-\Delta E/T_e)/T_e^{1/2}$. For the present plasma the electron temperatures are always smaller than the threshold energies E_s (capture energy) and ΔE (energy gap). The decrease of the respective excitation rates is therefore exponential with decreasing temperature. Moreover, MHD calculations show that outer regions with lower temperature correspond also to lower density resulting in a further decrease of excitation processes. The exponential decrease with T_e together with the decreasing density in the outer regions lead to negligible contributions from the outer plasma. The present selection of emission lines of H-, He-, and Li-like ions mainly originate from the hottest and densest part. Space resolved spectroscopy [23] has demonstrated this experimentally.

The influence of plasma regions with lower T_e can therefore be mainly due to photoabsorption, however, photoabsorption of satellite transitions in outer cold plasma sheaths reported in Ref. [24] cannot be responsible for the absence of satellite spectra in the 200 Pa case. Experiments clearly show the simultaneous absence of Li-like and He-like satellites. For He-like satellites the absorbing ground states are the single excited He-like $1s2l$ levels, which do not give rise to any important optical thickness effects.

V. DIELECTRONIC SATELLITE SPECTRA AND RECOMBINATION CONTINUA

Although the use of the parameter development for electron temperature and electron density obtained from the plasma bag calculations leads to a qualitative explanation of the observed ratios for the W and the Ly$_\alpha$ line, the differences concerning the intensity of satellites and the occurrence of recombination continua for the two different gas pressures, there are still discrepancies in the line intensity of the dielectronic satellites and the forbidden Y line especially in the 400 Pa case, namely, the satellites and the forbidden Y line have too low intensity. Higher satellite intensity can of course be obtained by lower temperatures at maximum compression. However, this will be in considerable disagreement with the Ly$_\alpha$- and W-line intensities. From purely spectroscopic argument it therefore seems that in the case of 400 Pa after maximum compression a phase with low electron temperature and higher electron density than predicted by the plasma bag calculations takes place, which gives rise to long lasting recombination effects. In order to meet the experimental intensities of the satellites and recombination continua, densities not much lower than or the same as the maximum values are required. Otherwise the time integrated intensity would be too low to compare with the experimental spectra. Furthermore, a lower electron temperature of about a factor of 2 is required. Otherwise the time integrated intensity of the dielectronic satellites would be too low due to the exponential behavior $\exp(-E_s/T_e)/T_e^{3/2}$ for the dielectronic capture.

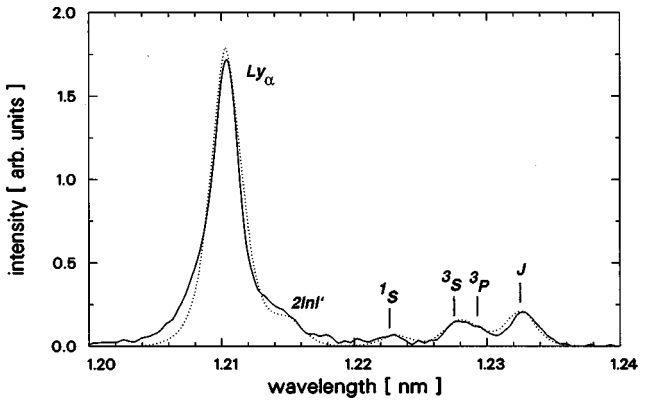

FIG. 6. Detailed spectrum modeling of the He-like $2lnl'$-$1snl''$ satellites close to the H-like Ly$_\alpha$ transition for 400 Pa gas pressure. This spectral interval has not been fitted separately but is a result of the parameter dependence given in Table II, which was also chosen for the total fit shown in Fig. 4(b).

As the satellite emission and the Ly$_\alpha$ intensity is of central interest we performed detailed transient spectra modeling of the He-like satellites $2l2l'$-$1s2l'$.

Keeping the behavior of plasma parameters as outlined in Fig. 3, we arrive at the corrected values for the maximum compression and the expansion phase. These corrected values are given in parentheses in Tables I and II. With the help of this few corrections a favorable agreement for various line intensity ratios is achieved, as is already shown. Figure 6 shows the details of the satellite spectrum close to the Ly$_\alpha$ line. There is a good agreement also in every spectral detail based on the time-dependent plasma parameters given in Tables I and II.

The predictions concerning the evolution of the plasma parameters based on the spectroscopic considerations, namely, the existance of a strong recombination radiation after maximum compression, is supported by time resolved measurements of the total K-shell emission and streak images of the plasma dynamics in the visible range.

Figure 7 shows the total K-shell emission measured with a MCP covered with a 10 μm Al foil. For the 400 Pa gas pressure a longer lasting wing in the emission profile is obtained, which is not so pronounced in the case of 200 Pa. As the MCP is covered with an Al foil and its direction of observation coincides with those of the high resolution x-ray spectrometer the time-dependent MCP measurements correspond to those from the time integrated x-ray spectrometer. To correlate the time dependent MCP signals with the evo-

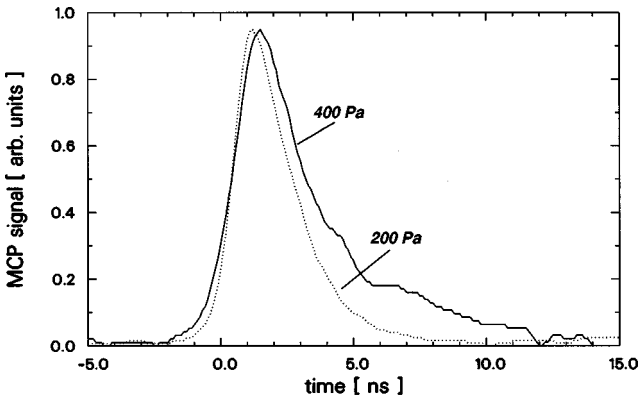

FIG. 7. Experimental time-dependent total emission for the 400 Pa and 200 Pa gas pressures.

lution of the emission lines and the continua, Figs. 8(a) and 8(b) show the time-dependent emission of the W, Y, and Ly_α lines, of the H-like photorecombination continuum (the selected wavelength interval was between 1.0 and 1.05 nm) and the He-like photorecombination continuum (selected wavelength interval between 0.85 and 0.9 nm) taking into account the absorption in the 10 μm Al filter.

Based on these calculations the asymmetric form of the x-ray MCP signal can be referred to recombination processes in the plasma. At the cooling phase the amount of H-like ions and nucleons stays high and the radiation resulting from recombination processes forms long lasting wings in the

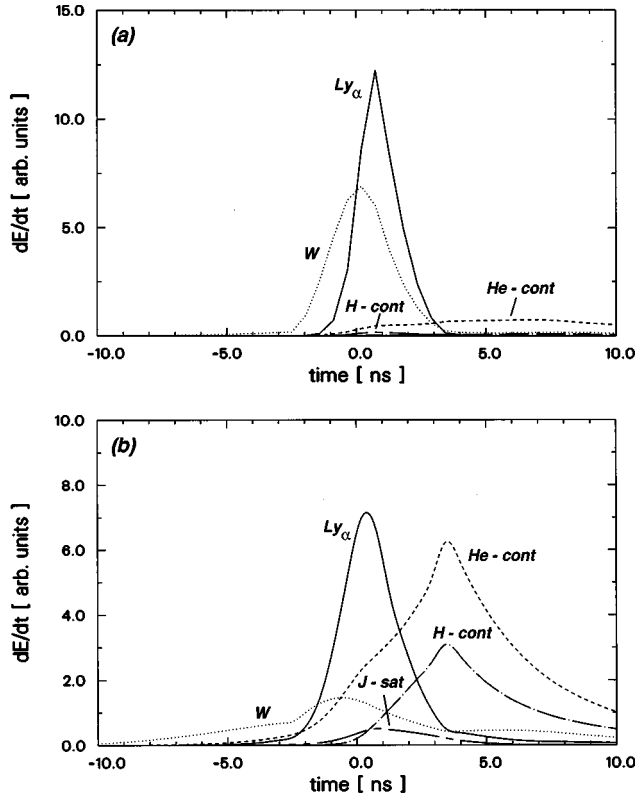

FIG. 8. (a) Calculated time-dependent emission of different lines and for the recombination continua for the plasma parameters given in Table I for the 200 Pa case. (b) Calculated time-dependent emission of different lines and for the recombination continua for the plasma parameters given in Table II for the 400 Pa case.

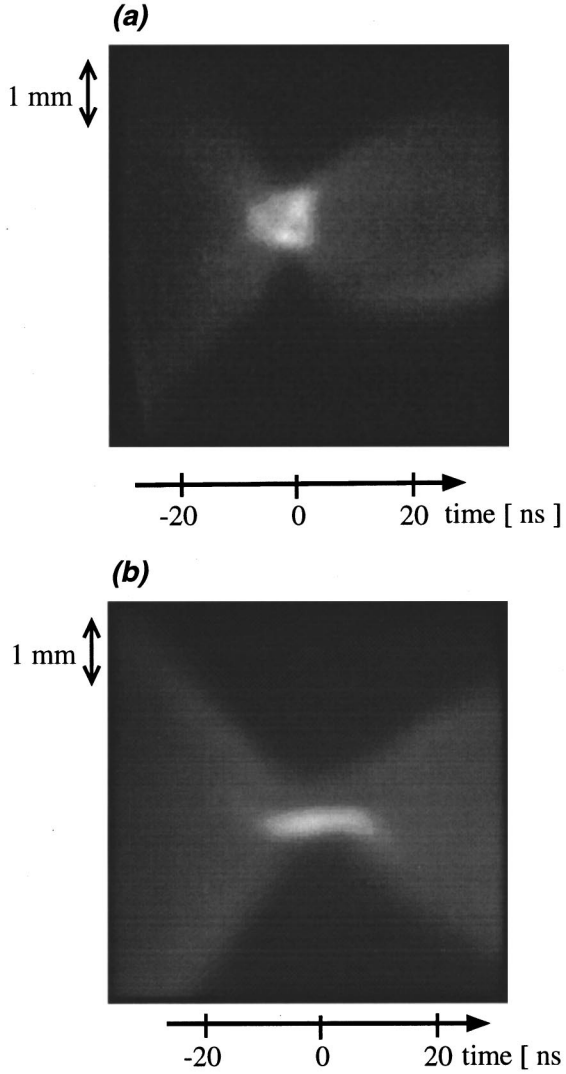

FIG. 9. (a) Streak image of the collapsing and expanding plasma layer in a discharge with 200 Pa neutral gas pressure. (b) Streak image of the collapsing and expanding plasma layer for the 400 Pa case.

x-ray emission. In the case of the 400 Pa experiment the wing has a higher intensity, because the electron density after maximum compression stays at a higher level than in the 200 Pa case. For 200 Pa the expansion of the plasma is faster, which is connected with a more rapid decrease of the electron density.

This different behavior of the plasma dynamics in the decay phase is supported by streak measurements of the plasma layer which are shown in Fig. 9. In the low pressure case the duration of the high compression state is lower than in the 400 Pa case. The plasma expands almost elastically for 200 Pa whereas at the higher pressure value it stays longer on the axis and has a lower expansion velocity. This is in agreement with the similarity considerations for the MHD, which suggest a velocity of the plasma layer v_s scaling according $v_s \propto I_0/(p^{1/2}a)$ [13].

Furthermore, the streak images support a higher maximum compression κ in the 400 Pa case. κ is defined as the ratio of density of neutral gas atoms to the maximum ion number density in the pinch phase. Using the numerical values for the electron density shown in Tables I and II and the

numerical values for the degree of ionization taken from Figs. 5(a) and 5(b) the compression is given by $\kappa \simeq 60$ for 200 Pa and $\kappa \simeq 100$ in the 400 Pa case. The minimum diameter of the pinch plasma observed in the visible range is lower in the 400 Pa case, indicating a higher compression of the pinch plasma.

Finally it should be noted that the results for the electron temperature from the spectroscopic considerations are also in agreement with the scaling law mentioned above. The temperature is assumed to scale according to $T_e \propto I_0^2/(pa^2)$. Using the numerical values for the current (270 kA for 400 Pa and 250 kA for 200 Pa) the maximum electron temperature for 200 Pa is assumed to be higher by about a factor of 1.7 compared to the 400 Pa case. Taking the numerical values given in Tables I and II for the maximum electron temperature this factor is about 1.5. A simple scaling law for the ion density according to $n_i \propto p$ is not verified quantitatively by the spectroscopic investigations. The model calculations presented lead to a ratio of maximum ion number density of about 3.3 comparing the 400 Pa to the 200 Pa case, whereas the scaling law would predict a factor of 2.

The zero-dimensional simulations of the *K*-shell emission spectra make use of an appropriate choice of the pinch plasma parameters assuming a homogeneous plasma. However, in a real plasma gradients in density and temperature in radial direction occur due to finite transport coefficients as described, e.g., in Ref. [25] where a one-dimensional simulation of a dense pinch plasma is presented. The most important contribution to the inhomogeneity of the plasma parameters will occur due to the process of thermalization of the kinetic energy of the ions when the plasma layer of the compression phase reaches the axis. This process leads to a reflected shock wave running outward in radial direction. Due to finite ionization time a smaller radius for hydrogenlike line emission is expected compared to the heliumlike line emission. In this sense the zero-dimensional approach overestimates the number of ions emitting hydrogenlike line radiation, especially in the present case where the pinch lifetime and the ionisation time from the heliumlike to the hydrogenlike level are of the same order of magnitude. However, this failure of the zero-dimensional approach can be compensated by a proper choice of density or confinement parameter which will not differ substantially from the real radial averaged density. So the zero-dimensional simulations provide reasonable estimations of the plasma parameters.

VI. CONCLUSION

The dynamics of neon pinch plasmas has been investigated theoretically and experimentally for two sets of device parameters, essentially for different neutral gas pressures and almost the same pinch current. These two sets lead to qualitatively different emission spectra.

A multifold use of spectroscopic analysis was developed and demonstrated which exceeds the common approach of using spectroscopy as a simple postprocessor of gas dynamic or MHD calculations.

An overall transient fitting of highly resolved, time integrated *K*-shell emission spectra leads to a good agreement not only when comparing resonance lines but also when considering details of dielectronic satellite spectra. Stationary models were shown to fail to explain the observed characteristic differences in the emission spectra for the two neutral gas pressures.

The transient spectra modeling allows us to estimate the evolution of the plasma parameters leading to an electron temperature of $T_e^{\max} \simeq 530$ eV and an electron density of $n_e^{\max} \simeq 2.5 \times 10^{19}$ cm^{-3} for the 200 Pa case at the instant of maximum compression. The respective values for the 400 Pa case are given by $T_e^{\max} \simeq 340$ eV and $n_e^{\max} \simeq 8.5 \times 10^{19}$ cm^{-3}.

These numerical values resulting from the model calculations are in agreement with scaling laws $T_e \propto I_0^2/(pa^2)$ and $n_e \propto p$ which are based on similarity considerations. These scaling laws predict a lower temperature and a higher density when increasing the neutral gas pressure keeping the current and the anode radius constant. The connection of the device parameters and the plasma parameters—here done for two sets of device parameters—allows the tailoring of the transient pinch plasma dynamics. This is important for basic studies of transient processes in plasmas as well as for the design of pinch plasmas as laboratory scale x-ray sources for different applications.

The detailed analysis of dielectronic satellite spectra predicts a long lasting emission after maxiumum compression for the higher neutral gas pressure. This prediction has been confirmed independently by time resolved analysis of the total emission and time and space resolved optical streak camera measurements. The predictive character of the dielectronic satellite spectra concerns not only the determination of the plasma parameters but also the qualitative type of emission after maximum compression. This is of importance for the understanding of the pinching process, especially because the above method is of general use and not connected to the specific type of experiment presented here.

ACKNOWLEDGMENTS

Parts of this work have been supported by the Deutsche Forschungsgemeinschaft (DFG) under Contract Number He 979/17 and the International Atomic Energy Agency Vienna (IAEA).

[1] N. R. Pereira and J. Davis, J. Appl. Phys. **64**, R1 (1988).
[2] J. J. Rocca, V. Shylaptsev, F. G. Tomasel, O. D. Cortazar, D. Hartshorn, and L. A. Chilla, Phys. Rev. Lett. **73**, 2192 (1994).
[3] C. Steden and H. J. Kunze, Phys. Lett. A **151**, 534 (1990).
[4] H. J. Shin, D. E. Kim, and T. N. Lee, Phys. Rev. E **50**, 1376 (1994).
[5] R. W. Clark, J. Davis, and F. L. Cochran, Phys. Fluids **29**, 1971 (1986).

[6] J. Davis, J. Giuliani, M. Mulbrandon, and F.L. Cochran, in *Dense Z-Pinches*, edited by Malcolm Haines and Andrew Knight, AIP Conf. Proc. No. 299 (AIP, New York, 1994), p. 112.
[7] S. J. Stephanakis *et al.*, IEEE Trans. Plasma Sci. **16**, 472 (1988).
[8] K. G. Whitney, J. W. Thornhill, J. P. Apruzese, and J. Davis, J. Appl. Phys. **67**, 1725 (1990).
[9] J. W. Thornhill, K. G. Whitney, J. Davis, and J. Apruzese, J. Appl. Phys. **80**, 710 (1996).
[10] K. G. Whitney *et al.*, Phys. Rev. E **50**, 2166 (1994).
[11] J. W. Mather, in *Methods of Experimental Physics, Plasma Physics*, edited by H. R. Griem and R. H. Loveberg (Academic Press, New York, 1971), Vol. 98, p. 187.
[12] D. Rothweiler, Ph.D. thesis, Rheinisch Westfälische Technische Hochschule Aachen, 1994.
[13] K. Bergmann and R. Lebert, J. Phys. D **28**, 1579 (1995).
[14] V. A. Boiko, A. V. Vinogradov, S. A. Pikuz, and A. Ya. Faenov, J. Sov. Laser Res. **6**, 85 (1985).
[15] A. H. Gabriel, Mon. Not. R. Astron. Soc. **160**, 99 (1972).
[16] F. B. Rosmej and O. N. Rosmej, J. Phys. B **29**, L359 (1996).
[17] D. Duston and J. Davis, Phys. Rev. A **21**, 1664 (1980).
[18] O. N. Rosmej and F. B. Rosmej, in Ref. [6], p. 560.
[19] O. N. Rosmej and F. B. Rosmej, Nucl. Instrum. Methods Phys. Res. B **98**, 37 (1995).
[20] V. V. Vikhrev and S. I. Braginski, Rev. Plasma Phys. **10**, 425 (1986).
[21] R. Lebert, W. Neff, and D. Rothweiler, X-Ray Sci. Technol., **6**, 107 (1996).
[22] V. F. Dyachenko and V. S. Imshennik, Zh. Eksp. Teor. Fiz. **56**, 1766 (1969) [Sov. Phys. JETP **29**, 947 (1969)].
[23] S. Morita and J. Fujita, Appl. Phys. Lett. **43**, 443 (1983).
[24] S. Kienle, F. B. Rosmej, and H. Schmidt, J. Phys. B **28**, 3675 (1995).
[25] V. F. Dyachenkov and V. S. Imshennik, Rev. Plasma Phys. **6**, 447 (1975).